Electronic Transport Through Odd-Even Methylenic Spacers Connected to an Aromatic Ring.

[a] Moreira, A.C.L ; V. Lenzi [b] ; L. S. Marques[b]
[a] Núcleo Interdisciplinar em Ciências Exatas e da Natureza - NICEN
Universidade Federal de Pernambuco, 50740-540, Recife/PE, Brasil;
[b] Centro de Física das Universidades do Minho e do Porto,
Universidade do Minho, 4710-057, Braga, Portugal

Abstract

In this work we propose a theoretical study of charge transport through a nanostructure composed by a methylenic bridge with a phenyl ring at the end, attached between a small silicon cluster in the bottom and a small lead cluster at the top. We use the Non Equilibrium Green Function theory (NEGF-theory) approach with the electronic structure treated at the density functional theory (DFT) level, and model the self energy with the wide band limit approximation. By varying the size of the methylenic bridge from two to five carbons, we show that a geometrical odd-even effect appears in charge transport for cryogenic temperatures, while it is suppressed at room temperature. Such phenomenon was studied by Combinining MD simulations with ab-initio NEGF transport calculations, thus *accounting for the thermal effects.. Our theoretical approach reveals the role of avoided-crossing effect on system conductance, occurring only for some alkyl bridge lengths.*

1. Introduction

Nanoscale organic electronic devices are amongst the strongest candidates for novel miniaturized electronic components. Understanding and controlling how electrons cross a single molecule placed between two substrates (or tips) not only represents a problem of great scientific interest, but is also fundamental to guide the devising of next-generation electronic devices at the nanoscale level. The first modern proposal of a single molecule as an electronics device was presented in 1974 by Aviram and Ratner [1], which suggested that molecules composed by an electron donor (D) species connected to an electron acceptor (A) group through a methylenic bridge (B) could act as current rectifiers. Nowadays, the technological potential of molecular electronic devices is clear and their exploration is only at the beginning: not only restricted to DBA systems, a wide variety of functional molecules exists in nature that, together with their anomalous and unexpected effects, can be used in the formulation of new functional devices [2-7]. One of these anomalous effects, with scientific interest, is the so called even-odd effect, in which the parity of the number of atoms/species in the bridge moiety directly affects the conductivity. The odd-even effect has been observed

in many different systems, from metallic nanowires [8-10] to organic molecules [11-13].

Theoretical studies of this phenomenon in monovalent metallic nanowires have been presented by many authors [8-10, 14]. In ref. [9], for example, the authors found that in sodium nanowires with an odd number of atoms the charge transport has a resonant character and displayed a robust quantization of conductance (G), with G near the quantum of conductance (G0) per transmission mode. Conversely, for even-numbered Na nanowires the transport mechanism is off-resonance and the conductance is smaller than (G0). In this case, the authors suggest that the key aspects for the observed even-odd behavior are both the sharp tip structure and the charge neutrality of monovalent metallic wires. The same even-odd oscillation as function of number of atoms in the chain was observed by Nieminen and coworkers [14] using Friedel sum rule and stressing the influence of the contact geometry, thus recommending to solve self consistently an extended molecule made by the wire itself and parts of the contact regions included in the system.

From an experimental point of view, Smit and coworkers [10], using mechanically controllable break junctions, recorded traces of conductance during the pulling process and detected an oscillatory behavior of conductance during the formation of monoatomic chains, with the conductance for the even-numbered chains smaller than G_0. This behavior was not only observed for monovalent gold, but also for other metals such as platinum and iridium, hence suggesting that this might be a universal feature.

Even-odd effect are not only restricted to metallic nanowires, but have also been found and theoretically studied in organic systems [7, 12, 15, 16]. In Ref. [11] for instance, a pronounced odd-even effect has been observed in a biphenyl system with *n*-alkanethiols acting as linkers (*n* being the number of (CH_2) groups in the alkanethiol chain) deposited on a gold surface, with a sulfur atom acting as a molecular alligator clip. The authors investigate the microscopic origin of these odd-even effects in terms of the local sulfur-gold bonding geometry by employing first-principles calculations and conclude that the even-odd effects may be understood by means of geometrical aspects: on one side, the dependence in the hybridization of the sulfur docking group at the sulfur-gold interface; on the other side, the torsion angle between the phenyl moiety and the alkanethiol linker.

Similarly, Whitesides and coworkers [7] observed differences in current density between *n*-alkanethiols with odd and even numbers of methylenes and showed that even-numbered alkanethiols typically have higher current density than odd-numbered ones. Despite this difference, both cases exhibit an exponential decrease in current density with increasing chain length.

The same trend was detected by Toledano and coworkers [13] in a system composed by a phenyl ring attached to a methylenic bridge binded to a silicon surface, and with the presence of a capping lead surface above the phenyl. They observed that, at low temperatures, for ethyl (*n*=2 CH_2 groups) and butyl (n=4) bridges the current density is greater than for propyl (*n*=3) and pentyl (*n*=5) ones. The authors explain the change in the current density between *n*=3 and *n*=4 by means of the different orientation of the phenyl ring for different bridges: while for even bridges the orientation is such that it reduces the overlap between the molecule and the lead substrate, for odd ones the barrier is increased, hence contradicting the exponential decay behavior with increasing chain length. Most interestingly, this inversion between $n = 3$ and $n = 4$ is not observed at room temperature (300 K). Whereas the authors advance the hypothesis that this is related to a decrease in the angle between the phenyl ring and methylenic bridge, a microscopic detailed description of this effect is still open and a full understanding is still missing.

This work aims at providing a theoretical explanation of precisely this phenomenon: how is it possible that, four carbons in the bridge conducts better than three and why such inversion is not observed at room temperature. In this regard, a theoretical model will be introduced in section 2, describing the different ingredients of our approach: transport theory (section 2.1), the computational approach for the electronic structure of the systems (section 2.2), molecular dynamic calculations to consider temperature effects (section 2.3) and the model self-energy (section 2.4). In section 3 we will discuss the results, while conclusion and future work will be addressed in section 4. We will show that the odd-even behavior and its suppression at high temperatures can be easily understood in the framework of a simplified model self-energy within a wide band limit approximation and a simple Lorentzian-like transmission.

2. Theory

2.1 Quantum transport Theory

The electronic transport through a single molecule placed between two substrates, denoted as *Top* and *Bottom*, will be studied using a model self-energy approach to calculate the transmission function. If the strength of the interaction between the molecule and the substrates is large, substrate-molecule hybridization occurs and the molecular levels are shifted and broadened [17, 18]. In this case of strong coupling limit, the transport is coherent, and the electronic current is given by [19-21]:

$$I = \frac{2e}{h}\int_{-\infty}^{+\infty} T(E)\left(f_T(E) - f_B(E)\right) dE \quad . \tag{1}$$

In Eq. (1), $f_T(E,\mu_T)$ and $f_B(E,\mu_B)$ are the Fermi distribution functions for the top and bottom substrates, respectively, and $T(E)$ is the total transmission function, usually obtained using the non interacting version of the Non-Equilibrium Green´s Function (NEGF) approach expressed as [19, 21, 22]:

$$T(E) = Tr\left[\tilde{\Gamma}_T(E)\, \tilde{G}_M^r(E)\, \tilde{\Gamma}_B(E)\, \tilde{G}_M^a(E) \right] \quad , \tag{2}$$

with *Tr* denoting the trace. All quantities in brackets are matrices whose dimensions correspond to the number of elements of the atom-centered basis set that spans the system – usually an extended molecule, that is, the molecule itself with some atoms of the contact (electrodes) coupled at the ends. In Eq. (2), $\tilde{\Gamma}_T(E)$ and $\tilde{\Gamma}_B(E)$ are the top and bottom coupling of the molecule to the substrates, while $\tilde{G}_M^r(E)$ and $\tilde{G}_M^a(E)$ are the retarded and advanced Green´s functions, i.e., the propagators through the molecule region, which are related by $\tilde{G}_M^r(E) = \left(\tilde{G}_M^a(E)\right)^\dagger$. Note that due to the coupling of the molecule with the semi-infinite systems,the Green´s function of the full system (i.e., the extended-molecule plus semi-infinite substrates) evolves accordingly to an effective Hamiltonian ($\tilde{H}_0 \rightarrow \tilde{H}^{eff} = \tilde{H}_0 + \tilde{\Sigma}^r(E)$), in the form:

$$\tilde{G}_D^r(E) = \left[E\tilde{S} - \left(\tilde{H}_0 + \tilde{\Sigma}^r(E)\right)\right]^{-1}, \tag{4}$$

where $\tilde{\Sigma}^r(E) = \tilde{\Sigma}_T^r(E) + \tilde{\Sigma}_B^r(E) = \left(\tilde{\Delta}_T(E) + \tilde{\Delta}_B(E)\right) - \frac{i}{2}\left(\tilde{\Gamma}_T(E) + \tilde{\Gamma}_B(E)\right)$ is the total retarded self-energy due to the top and bottom substrates contributions. The imaginary terms are given by $\tilde{\Gamma}_{T/B}(E) = -2\,\mathrm{Im}[\tilde{\Sigma}_{T/B}^r(E)]$ and the real ones by $\tilde{\Delta}_{T/B}(E) = \mathrm{Re}[\tilde{\Sigma}_{T/B}^r(E)]$. Note that while the real part of the self-energy shifts the level ε_α, the imaginary part is associated with the broadening and finite lifetime of this level. Finally, $\tilde{S}$ is the overlap matrix, which is the identity matrix for the case of an orthonormal basis set. In next sections, a model self energy will be developed, united with a simplified description of the semi-infinite substrates.

2.2 Electronic Structure

The description of the electronic transport through the molecular systems was made by adopting the extended molecule model depicted in Fig. 1. Since a perfect control of the contacts between the substrates and the molecules is still an experimental challenge, an assumption has to be made for modeling purposes. Without loss of generality, we will employ a local model for the contacts, in which a finite part of each substrate is added to describe these junctions [23-25]. Therefore, the silicon and lead substrates are modeled by a finite amount of atoms, with a silicon atom covalently bound to the edge carbon atom of the methylenic bridge and a layer of lead atoms near the phenyl ring as shown in figure 1. For each extended molecule Si_5-C_nBz with *n* the carbons in the bridge varying from 2 to 5 and hydrogens omitted for clarity, geometry optimizations and single point energy (SPE) calculations were performed at the DFT level using the Gaussian 09 program [26]. Similar to ref. [27], for geometry optimization of the molecular system we adopted the following protocol: (i) with the B3LYP hybrid functional and the 6-31G+(d, p) basis sets a small cluster containing five silicon atoms was obtained, as shown in Figure 1a; (ii) using the B3LYP hybrid functional and the 6-31G+(d, p) basis a full optimized geometry for the extended molecule Si_5-C_nBz was obtained, as shown in Figure 1b; (iii) using B3LYP hybrid functional and the LANL2DZ basis sets the optimized geometry of a lead cluster containing seventeen atoms disposed in two layers (to avoid an artificial flat conformation [28]) was obtained, as shown in Figure 1b; (iv) the extended molecule obtained in point (iii) was joined with just one layer of the lead cluster, keeping the phenyl´s center of mass aligned to the lead cluster center of mass and with the distance

L (see figure 1c) between the highest Si-atom and the lowest lead atom set as the experimental values obtained with ellipsometry techniques in reference [13] (see table 1); (v) finally, the system was re-optimized freezing all silicon and lead atoms and a SPE calculation with the optimized geometry was performed using the B3LYP hybrid functional along with the LANL2DZ basis set for lead atoms, and 6-31G+(d, p) basis set for the remaining ones.

Table 1: Distance between lead and silicon substrate (L) used in the electronic structure calculation

System	Si5-C2Bz-Pb10	Si5-C3Bz-Pb10	Si5-C4Bz-Pb10	Si5-C5Bz-Pb10
Distance: L (nm)	9.6	10.2	10.7	11.2

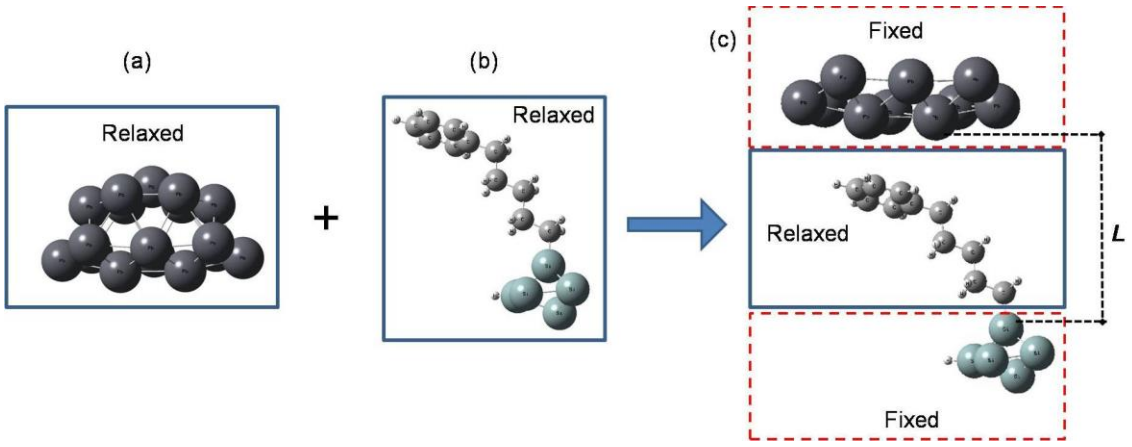

Figure 1: Schematic view of the procedure for obtaining the electronic structure for C5Bz. The procedure is the same for all systems considered.

The inclusion of the electric field in the single point energy calculations, was also considered, but due to the very small variation of the eigenvalues and eigenvectors (see support information) it was omitted for the sake of simplicity.

2.3 Molecular Dynamics simulations.

As reported in reference [13], the key aspect in the systems described in previous section is the inversion in the magnitude of the electrical current between four carbons in the bridge and three carbons in the bridge. Despite having a longer bridge, for cryogenic temperatures (T → 0K), the current for four carbons in the bridge is higher than for three carbons. This behavior disappears back at room temperature (300

K) and the authors attribute this inversion to changes in the P-M angle due to the temperature increase. Thus, since DFT calculations are made at zero Kelvin, to include temperature effects, molecular dynamic calculations were performed using LAMMPS [29, 30]. The REAXFF forcefield [31], and the parametrization from Soria et al. [32] developed for silicon surfaces grafted with organic molecules was employed.

Silicon 111 surfaces were simulated as 3-layer thick slabs, one side of which was functionalized with phenyl molecules. Under full periodic conditions, an 8x8 supercell was created and 50 % coverage was considered (see figure 2). A total of 32 phenyl molecules were placed upon the substrate, disposed according to a checkerboard pattern. A vacuum layer of 2 nm was added in the z direction to avoid interactions between periodic images.

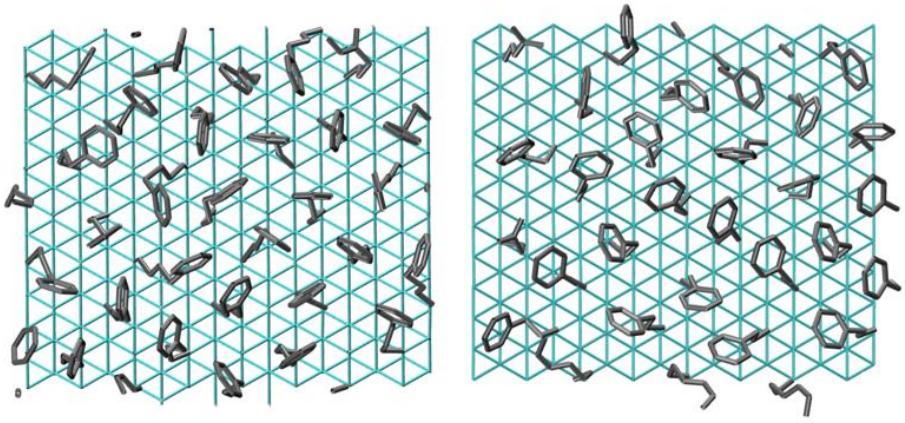

Figure 2: Top view of the silicon substrates grafted with C4Bz (left) and C3Bz (right) phenyl molecules, taken at 6 K. Silicon atoms are in cyan, while carbons are in gray. Hydrogens were omitted for clarity. For C4Bz and even molecules, ring planes tend to be parallel with respect to the line of sight.

A time step of 0.5 fs has been used. All simulations were performed under NPT conditions, with a Nosé-Hoover thermo and barostat [33, 34] with a damping factor of 25 fs and 250 fs, respectively. In all simulations pressure was kept fixed to 0 *atm*, and the barostat was applied in the x and y directions only.

The molecules were initially attached in their fully stretched conformation, thus, after a 20 ps initial heating phase, a 500 ps run at 600 K was performed to randomize conformations and provide independent initial configurations for lower temperature runs. Production runs were performed for 2 ns at cryogenic temperature (6 K) and room temperature (300 K) and the system state was saved every 5 ps for further analysis. Five independent replicas were considered for each system and temperature. Finally, results obtained within MD for room temperature were incorporated in subsequent *ab initio*

calculations to obtain the electronic structures and mean values for transmission function with a model self energy and calculate the electrical current.

2.4 Model Self Energy and Transmission

Once the electronic structure is available, the next step in our approach consists in model the self-energy. For this purpose, we assume a wide band limit approximation [21, 24] where the interaction with the semi-infinite substrates are described by a purely imaginary energy independent self energy, i.e. $\tilde{\Delta}_{T/B}(E)=0$ and $\tilde{\Gamma}_{T/B}(E)=\tilde{\Gamma}_{T/B}=-2\,\mathrm{Im}[\tilde{\Sigma}^{r}_{T/B}]$. The term $\tilde{\Sigma}^{r}_{X}$ (X = T, B) runs over the top/bottom substrate atomic basis of the extended part of extended molecule [35-37]:

$$\tilde{\Sigma}^{r}_{X}=\frac{-i\Gamma}{2}\sum_{x\in X}\left|\bar{x}\right\rangle\left\langle\bar{x}\right| \quad , \tag{5}$$

with $\left|\bar{x}\right\rangle=\sum_{y}S^{-1/2}_{xy}\left|y\right\rangle$ being an orthonormal basis [38] that obeys $\langle\bar{x}|\bar{y}\rangle=\langle\bar{y}|\bar{x}\rangle=\delta_{xy}$ and indexing the top (X = T = lead atoms) and bottom substrate atoms (X = B = silicon atoms) of the extended molecule. The term $S^{-1/2}_{yx}$ is the *yx* element of the square-inverse of overlap matrix ($[\boldsymbol{S}]^{-1/2}$) and $\sum_{x\in X}\left|\bar{x}\right\rangle\left\langle\bar{x}\right|$ is the projection operator into the X-region ($\hat{P}_X$) in the orthonormal basis representation [38, 39]. This simple self energy model is nothing but a local absorption potential that mimics the semi-infinite substrate environment effects in a finite region [24, 35, 37] – the extended part of the EM.

We can go further and reduce computational cost if, instead of solving the eigenvalue problem of two non-hermitian Hamiltonians and finding a bi-orthonormal set of eigenvectors, we build the effective Hamiltonian ($\tilde{H}^{eff}$) using the unperturbed eigenvectors of the extended molecule (H_0) [40, 41]. This method gives good qualitative results for a simple Hückel model of an infinite linear chain [40], giving a fair amount of broadening of the resonant peaks and predicting correctly their position. This latter fact, united with the local model self-energy as defined in Eq. 5, captures the main physics of the system.

Let us then consider the set $|\bar{\alpha}\rangle$ of eigenvectors for H_0. Reminding that in an orthonormal basis set $|\bar{\mu}\rangle$ a Molecular Orbital (MO) $|\bar{\alpha}\rangle$ can be written as a Linear Combination of Atomic Orbitals (LCAO) ($|\bar{\alpha}\rangle = \sum_{\mu} \bar{C}_{\mu}^{\alpha} |\bar{\mu}\rangle$) where each MO is normalized such that $\langle\bar{\alpha}|\bar{\alpha}\rangle = \sum_{\nu,\mu} \bar{C}_{\nu}^{\alpha *} \bar{C}_{\mu}^{\alpha} \delta_{\nu\mu} = 1$, the projection of Eq. 5 into the unperturbed eigenvectors of H_0 results:

$$\tilde{\Sigma}_{X[\bar{\alpha}]}^{r} = -i\Gamma |\bar{\alpha}\rangle\langle\bar{\alpha}| \left[\sum_{x \in X} |\bar{x}\rangle\langle\bar{x}| \right] |\bar{\alpha}\rangle\langle\bar{\alpha}| = -i |\bar{\alpha}\rangle \Gamma_{X}^{\alpha} \langle\bar{\alpha}| \quad , \tag{6a}$$

with $\Gamma_{X}^{\alpha} = \Gamma \Omega_{X}^{\alpha}$ and,

$$\Omega_{X}^{\alpha} = \sum_{n \in X} \left| \bar{C}_{n}^{\alpha} \right|^2 = \sum_{n \in X} \left| \sum_{b \in All} S_{nb}^{1/2} C_{b}^{\alpha} \right|^2 . \tag{6b}$$

Equation 6a-b shows that for a specific eigenvalue (α) the level-broadening is dependent of the probability of finding the molecular orbital localized on the top substrate region and bottom substrate region, implying that the main contribution will come from states with significant coefficients of the LCAO expansion of the wave-function in these regions [35, 37]. Note that the orthonormal ($\bar{C}_{n}^{\alpha}$) and non-orthonormal (C_{b}^{α}) expansion coefficients are related by $\bar{C}_{n}^{\alpha} = \sum_{b} S_{nb}^{1/2} C_{b}^{\alpha}$, where the index *b* runs over all basis set functions of the full system (*b* ϵ *All*) and the index *n* involves only the basis set region of a specific substrate (silicon or lead). Thus, a non-null overlap can give small contributions to the level broadening, even if it occurs outside the substrate basis region,. With the self-energy as defined in Eq. 6a, the effective Hamiltonian – in the orthonormal basis $|\bar{\alpha}\rangle$ – is given by:

$$\hat{H}^{eff} = \hat{H}_0 - i\hat{\Gamma} = \sum_{\alpha} |\bar{\alpha}\rangle \left[\lambda_{\alpha} - i\left(\Gamma_{T}^{\alpha} + \Gamma_{B}^{\alpha} \right) \right] \langle\bar{\alpha}| \quad . \tag{7}$$

where $-i(\Gamma_T^\alpha + \Gamma_B^\alpha)$ can be viewed as the first order correction for the unperturbed eigenvalues (λ_α) in time independent perturbation theory. The first order correction is null for the states $|\bar{\alpha}\rangle$ and corrections in higher order for eigenstates and eigenvalues will be always null due to our choice of expansion using the eigenvectors of H_0. The Green´s function evaluation is straightforward and the transmission is written as [3, 19, 42]:

$$T(\lambda) = \sum_\alpha \frac{4\Gamma_T^\alpha \Gamma_B^\alpha}{\left(\lambda - \lambda_\alpha\right)^2 + \left(\Gamma_T^\alpha + \Gamma_B^\alpha\right)^2} \quad , \tag{8}$$

and, as expected, will be nonzero only if the state is delocalized, having non null weights in both regions of the substrate. Finally, we assume that in the chemical potential ($\mu_T = E_f + eV$, $\mu_B = E_f$) the voltage drops only at the extended molecule-lead interface [43].

3. Results

3.1 Geometry and Transmission for 0K

As discussed in previous sections, the main feature that defines the odd-even effect in a system is the change in geometrical aspects of the system as a result of the even or odd number of atoms contained in the bridge. In this section we discuss the geometrical aspects of the system and verify their influence in the MO's energies.

By looking at the optimized geometries for the Si-CnBz-Pb systems, with n between 2 and 5, we observed that the relative position between the phenyl ring and the lead surface varies significantly depending on the even or odd number of carbons in the methylenic bridge, as shown in figure 3a-b for C2Bz and C3Bz – and in a similar fashion for C4Bz and C5Bz. While for even carbons in the bridge, the angle (θ_{even}) between phenyl ring and the lead surface is around 85°, for an odd number of carbons in the bridge, θ_{odd} is around 25°. Clearly, for θ_{even} the outmost carbons in the ring are closer to the surface containing the lead atoms that for θ_{odd}. As a consequence, this geometric conformation – with the phenyl group almost perpendicular to the top (lead) surface – can be expected to be more favorable for transport since, in this situation, the occurrence of a higher overlap between the phenyl ring and the lead surface exist when

compared to the odd number of carbons in the bridge. Moreover, some MOs for systems with even n tend to have a higher probability to be delocalized through all the system, thus, resulting in higher values for the transmission function peak analyses. These geometrical trends agree with molecular dynamics simulations reported in reference [13].

Another important geometrical parameter the Phenyl-Methyl (P-M) angle φ as defined in figure 3c. This is an internal angle whose importance will appear when thermal effects will be added in the model. For the moment, the main aspect to consider is that, while for an even number of carbons in the bridge its value is 106.16° and 104.18° for *n*=2 and *n*=4, respectively, for odd number of carbons its value is 113.14° and 111.68° for *n*=3 and *n*=5, respectively. Thus, the difference between odd and even systems is small when compared with that of the θ angle and, unless some unexpected phenomenon involves this parameter, in principle it should not affect significantly the behavior of the system.

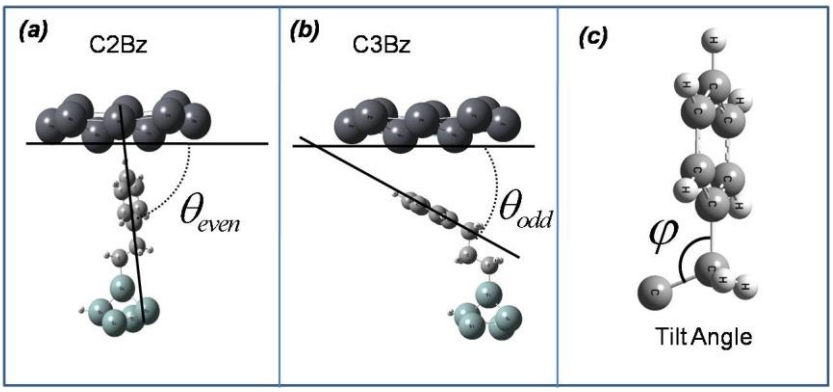

Figure 3: Difference in the relative positions between Pb-cluster surface and the phenyl ring for even and odd carbons in the methylenic bridge for: (a) n = 2 and (b) n = 3, as determined by the angle θ*. The same trend holds for n = 4 and n = 5. In (c) is shown the definition of Phenyl-Methyl (P-M) angle φ.*

The influence of conformation in the transmission function is shown in figures 4a-d where, for each system, the main MOs involved in the process are depicted in the inset. For the systems with an even number of carbons in the bridge the transmission improves , because the MOs involved in the transport process are more delocalized, with significant weights on both extremities of the extended molecule. Thus, for C2Bz and C4Bz, the LUMO+6 and LUMO+8 are the delocalized MOs responsible for the main peaks in the transmission (Figs. 4a and 4c), acting as ballistic channels for transport.

In the case of odd methylenic bridges (C3Bz and C5Bz), we have the opposite situation: MOs are more localized with no significant weights on both ends, increasing the asymmetry between the top and bottom couplings when compared with even methylenic bridges and hence decreasing the transmission, as shown in Fig. 4b and Fig. 4d for C3Bz and C5Bz, respectively. Note that, despite LUMO+6 and LUMO+7 are the transport channels in both systems (C3Bz and C5Bz), there is only one peak for C3Bz, as a consequence of the broadening effects that suppress the resolution of the almost degenerate eigenvalues of these MOs. For *X* = *Top*/*Bottom* and α = LUMO+*N*, with *N* = 6 and 8 [6 and 7], table 2 reports the Ω_X^α values (see Eq. 6b) and the relative eigenvalues (λ) all systems considered here.

Table 2: Ω_X *(with X = Top, Bottom) and eigenvalues* α=*LUMO+N (N=6, 8)*

Even Systems						
Ω_X^α	Ω_{TOP}^{LUMO+6}	Ω_{BOTTOM}^{LUMO+6}	*λ (a.u.)*	Ω_{TOP}^{LUMO+8}	Ω_{BOTTOM}^{LUMO+8}	*λ (a.u.)*
C2Bz	*0.0139*	*0.9522*	*-0.0783*	*0.9821*	*0.0101*	*-0.0763*
C4Bz	*0.0046*	*0.9828*	*-0.0775*	*0.9889*	*0.0041*	*-0.0756*
Odd Systems						
Ω_X^α	Ω_{TOP}^{LUMO+6}	Ω_{BOTTOM}^{LUMO+6}	*λ (a.u.)*	Ω_{TOP}^{LUMO+7}	Ω_{BOTTOM}^{LUMO+7}	*λ (a.u.)*
C3Bz	*0.0012*	*0.9367*	*-0.0783*	*0.9943*	*0.0013*	*-0.0778*
C5Bz	*0.0005*	*0.9888*	*-0.0782*	*0.9440*	*0.0006*	*-0.0763*

Results reported in table 2 show a high asymmetry in the sense that, for all systems, all MOs have a predominant localization at one end of the extended molecule. Thus, while for α=LUMO+6 we have $\Omega_{TOP}^\alpha \gg \Omega_{BOTTOM}^\alpha$ for even and odd systems, for α=LUMO+8 [α=LUMO+7] we have the opposite behavior ($\Omega_{TOP}^\alpha \ll \Omega_{BOTTOM}^\alpha$) for even [44] systems. However, despite of this apparent similarity, at least for *n* = 2 to 5, we always have $\min\{\Omega_{X-EVEN}^\alpha\} > \min\{\Omega_{X-ODD}^\beta\}$, where $\min\{\Omega_X^{\alpha/\beta}\}$ means the smaller value of $\Omega_X^{\alpha/\beta}$ (*X* = top or *X*=bottom) for a specific pair (α/β) of MOs working as transmission channels (in our case we have (α/β)→(LUMO+6 / LUMO+6) and (α/β)→(LUMO+8 / LUMO+7)).

Since we adopt a simple Lorentzian form for the transmission function (see eq 8), the term $\min\{\Omega_X^{\alpha/\beta}\}$ will dictate the peak values in the transmission function at the resonance, provided that $\max\{\Omega_X^{\alpha/\beta}\}$ do not vary significantly among each pair (α/β) of MOs – which is exactly the present case as shown in table 2. Thus, even with a small weight, the relative difference between $\min\{\Omega_X^{\alpha/\beta}\}$ for each pair of MOs shows that the geometric conformation for *n*-even is more favorable for tunneling between the phenyl ring and the lead cluster, when compared to systems with *n*-odd.

Integrating the transmission over the energy (as in Eq. 1) we obtain the electrical current for the four systems at 0 K, which is shown in Fig. 4e. Note that C4Bz (blue/triangle) conducts better than C3Bz (red/square) due to a more delocalized MO for systems with an even number of carbons in the bridge. Therefore, the main effect of the geometric conformation is to suppress the usual exponential decay as function of the length of the methylenic bridge, at least between $n = 4$ and $n = 3$. For positive bias voltage, these theoretical trends (geometry conformation and electrical current behavior) are empirically verified as reported in Ref. [13] for these systems by averaging over self-assemble monolayer (SAM) samples.

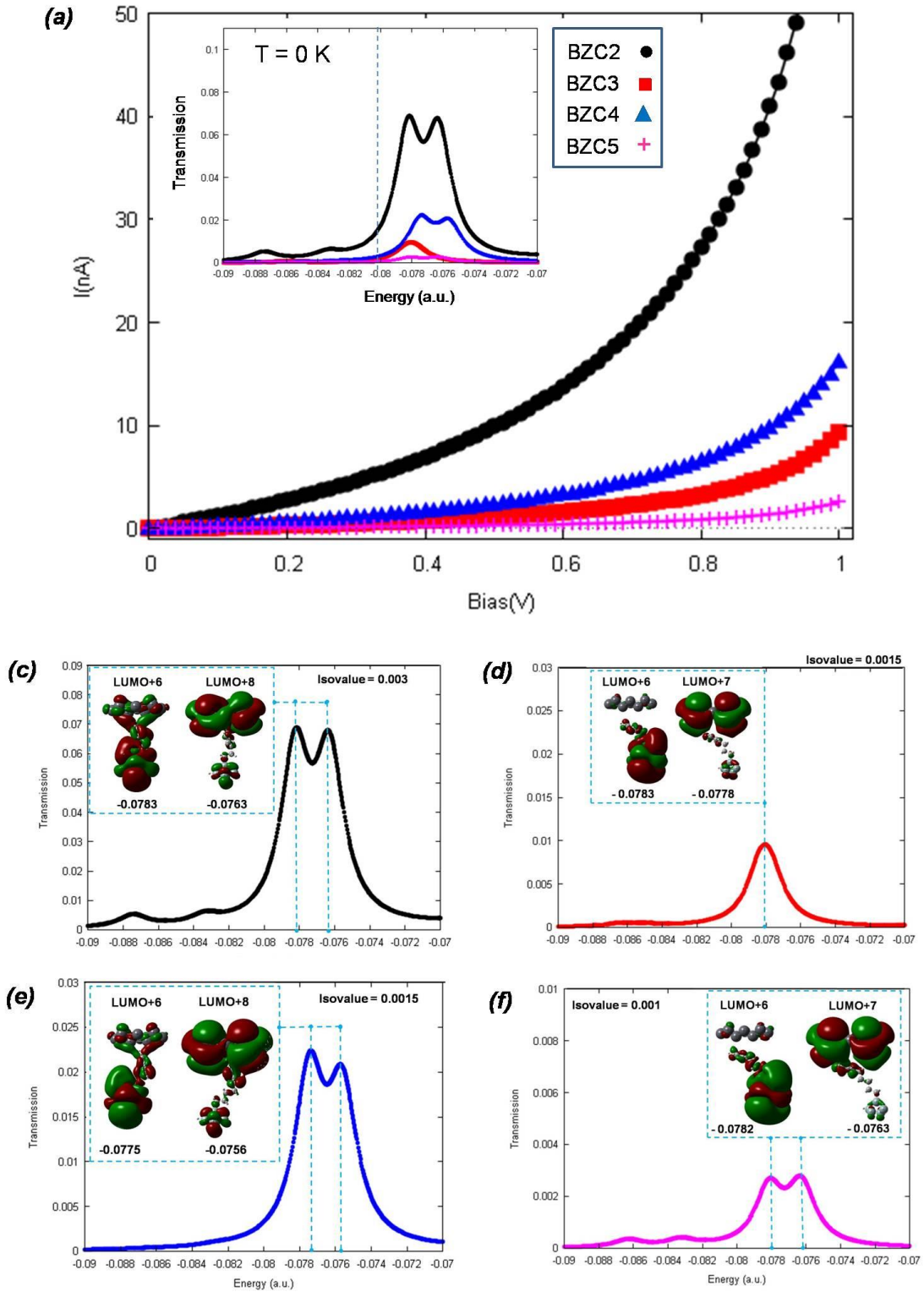

Figure 4: In (a) the electrical current for all systems and the transmission function plotted in the inset. Transmission function and the molecular orbital (and their eigenvalues) responsible by the peaks for (b) C2Bz, (c) C3Bz, (d) C4Bz and (e) C5Bz (isovalue = 0.0015).

It is important to stress that, unlike the (monovalent) atomic linear chains attached to narrow tips where a well-defined resonant electronic state appears at the Fermi level for odd chains [8-10] but not for even chains, there are no significant changes in the eigenvalues positions as function of the even-odd number of carbons in the bridge. This due to the fact that the phenyl ring breaks the even-odd effects of the energy alignment near the Fermi level, thereby we can conclude that the main contribution to the electrical current (at cryogenic temperature T→0K) comes only from the geometric conformation of the systems. This is not true however for T=300K where, a thermally induced MOs avoided-crossing effect [45-47] appears and needs to be addressed, as we will discuss in the next section.

3.2 Temperature's Induced Avoided Crossing Effects

From MD simulations it was possible to extract the probability distribution function $P(\varphi)$ for the P-M angle (φ) between the phenyl and the methylenic bridge, as shown in figure 5 only for n=3 and n=4. The temperature's effect on PM angle can be summarized as a slightly increase of its mean value, more specifically by an amount of 1~2 degrees from their cryogenic value (T= 6K). Despite the absolute of the peak value of φ obtained from MD (vertical dotted/blue line), and *ab-initio* methods do not coincide, both methods exhibit the same trends , i.e., $\varphi_{even} < \varphi_{odd}$, which remains true even at room temperature.

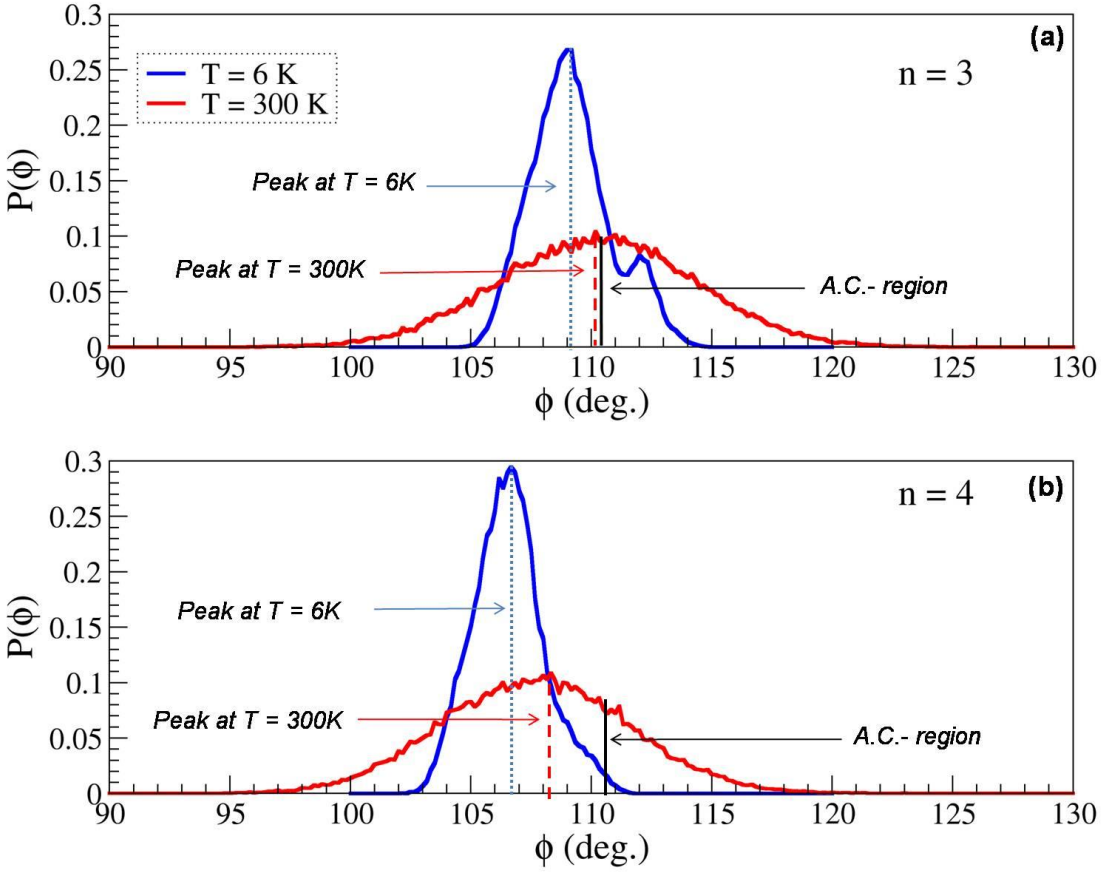

Figure 5: *Distribution function of the P-M angle at T→6K and T=300K for (a) n=3 (b) n=4. Vertical lines show the peak for: cryogenic temperature (T=6K), room temperature (T=300K) and the avoided-crossing value (A.C. region).*

We must stress here that numerical values obtained within MD simulations and DFT are not directly comparable, because in DFT we have an isolated extended molecule sandwiched on one side, while in MD a dense system was simulated – in the sense of a more realistic Self-assembled monolayer – without the lead top surface. So, it is expected that the exact values of φ and $\Delta\varphi = \varphi_{even} - \varphi_{odd}$ differ between MD and *ab initio* calculations. The explicit presence of the top lead surface modeled by a small cluster of *Pb* atoms in *ab initio* calculations makes $\Delta\varphi$ larger for *ab initio* calculations, however MD still keep the same trend $\Delta\varphi < 0$. Therefore, it is reasonable to consider that, due to the lack of covalent bonds between the phenyl ring and the *Pb*-cluster, the MD trends in $\Delta\varphi$ for the organic part of the system remains valid and can be accounted for posterior *ab initio* calculations.

Note also that, the increased thermal motion broadens the $P(\varphi)$ distribution as reported in figure 5a-b. Although these variations appear to be small, they have an important impact in the electron transmission: a small change in the P-M angle increases the probability to find the system into an avoided-crossing region, changing

the spatial localization of the molecular orbitals in such a way that the transmission function is greatly improved. To see this, we added to curves figure 5a-b the P-M angle necessary to bring the system to the avoided crossing (A.C.) region (vertical full/black line). This angle was calculated by adding to the MD criogenic peak value, the difference obtained in ab-initio calculations between the P-M relaxed value and the value to enter in the AC region, which is ~1º for C3Bz and ~4º for C4Bz (see figures 6b,d).

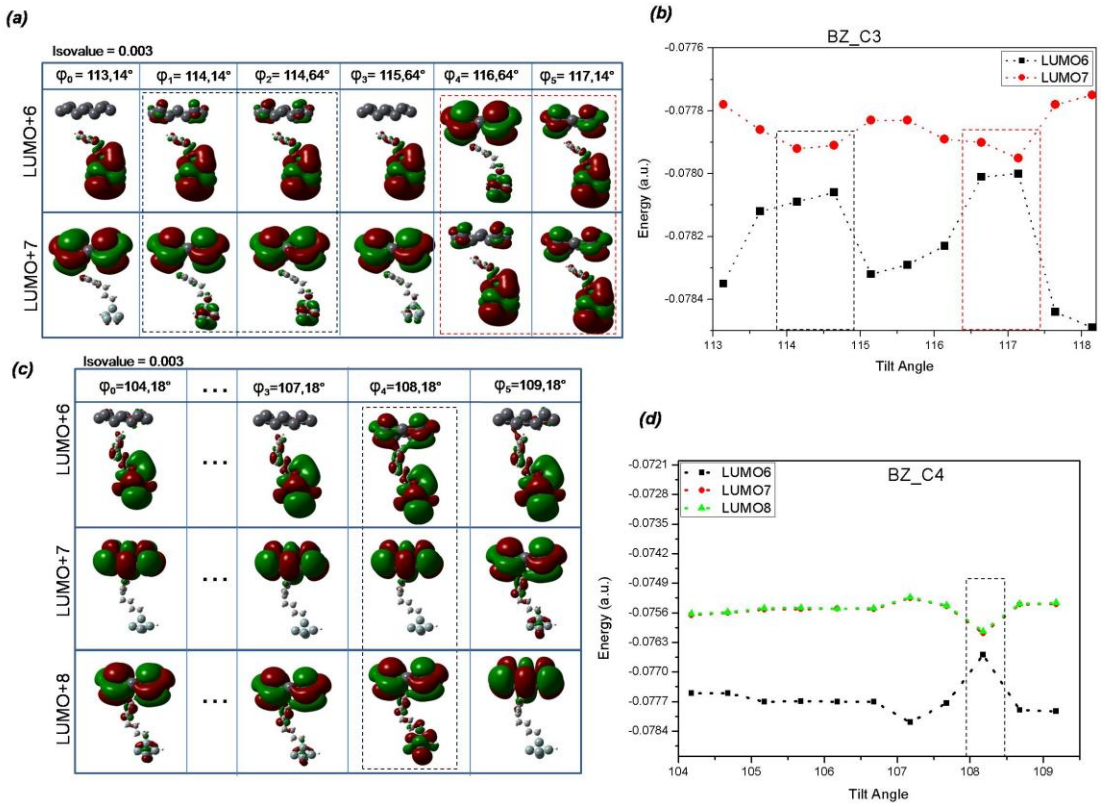

Figure 6: (a) Behavior of MOs LUMO+6 and LUMO+7 as function of φ for C3Bz. (b) Eigenvalues of LUMO+6 and LUMO+7 as function of φ for C3Bz showing the avoided crossing effect for φ=114.14° and φ=117.14°. (c) Behavior of MOs LUMO+6 and LUMO+8 as function of φ for C4Bz. (b) Eigenvalues of LUMO+6 and LUMO+8 as function of φ for C4Bz showing the avoided crossing effect for φ=108.18°.

The change in the spatial localization of the molecular orbitals associated to the energy levels involved in an avoided-crossing situation is reported shown in figure 6. The avoided crossing effect [48] can be understood considering a two level system $|\alpha_A\rangle$ and $|\alpha_B\rangle$ and their corresponding eigenvalues (λ_A and λ_B) associated to a non-perturbed Hamiltonian H_0. In the presence of a perturbation (W), the Hamiltonian can be written as $H=H_0+W$**.** The eigenstates and eigenvalues of H are given respectively by:

$$\begin{pmatrix} |\alpha_+\rangle \\ |\alpha_-\rangle \end{pmatrix} = \begin{pmatrix} +\cos\left(\frac{\alpha}{2}\right).e^{-i\frac{\delta}{2}} & \sin\left(\frac{\alpha}{2}\right).e^{+i\frac{\delta}{2}} \\ -\sin\left(\frac{\alpha}{2}\right).e^{-i\frac{\delta}{2}} & \cos\left(\frac{\alpha}{2}\right).e^{+i\frac{\delta}{2}} \end{pmatrix} \begin{pmatrix} |\alpha_A\rangle \\ |\alpha_B\rangle \end{pmatrix} \quad , \tag{9}$$

and

$$\lambda_{\pm} = \frac{1}{2}(\eta_A + \eta_B) \pm \frac{1}{2}\sqrt{(\eta_A - \eta_B)^2 + 4|W_{AB}|^2} \quad . \tag{10}$$

where δ is a phase factor, $\eta_A = \lambda_A + W_{AA}$, $\eta_B = \lambda_B + W_{BB}$ and $\tan\alpha = 2|W_{AB}|(\eta_A - \eta_B)^{-1}$, with $(0 \le \alpha \le \pi)$. Due to the effect of *W*, each one of the 'perturbed' eigenstates corresponds to a linear combination mixing the two pure original $|\alpha_A\rangle$ and $|\alpha_B\rangle$ states. However, an exchange between the features of the two original states will occur. This is especially true when the mixing parameter changes from its initial value ($\alpha = 0$ i.e., well before the interaction is switched-on) to its final limit ($\alpha = \pi$, i.e., long after that it has been switched-off). In this manner, at an avoided-crossing situation between two levels $|\alpha_A\rangle$ and $|\alpha_B\rangle$, the perturbation can dramatically modify the electronic distribution of the system. Thus, depending on the value of α (or η_A - η_B) in Eq. 9, two localized molecular orbitals (in different parts of the molecule as, for example, in the Top or Bottom regions) can mix to form two delocalized MOs. Hence, the avoided-crossing phenomenon may introduce a very peculiar situation for the overall electronic flow, since a perturbation $W = \delta H_0$, such as a variation of the P-M angle (φ), can modify two (non contributing) neighboring levels in such a way that, after the onset of *W*, the resulting MOs can suddenly become an important (delocalized) channel for charge transport [47].

This is exactly what happens with C_nBz systems when we consider thermal effects: the P-M angle (φ) changes and assumes values such that a small variation in the Hamiltonian ($W = \delta H_0$) can bring the system to a high probability of avoided crossing situation, as depicted in figures and 6a-d. It is worth noting that, according to the MD results shown in figure 5a for *n* = 3, the amount necessary to go from the peak of the distribution at a room temperature (red/dashed vertical line) to the A.C. region (black/full vertical line) is almost null, both being 'distant' only by an amount $\Delta\varphi \sim 1°$ from the value at cryogenic temperature. Considering this trend in *ab initio* calculations,

figure 6a-d shows that even small variations in the P-M angle can alter the eigenvalues of LUMO+6 and LUMO+7, because these MOs mix when the tilt angle lies around φ_{C1} =114.14° and φ =114.64°. A similar reasoning can be applied for φ_{C2}=116.64° to 117.14°. In this situation, the amount in φ to go from the peak value of $P(\varphi)$ at room temperature to the A.C. region is larger than the previous case – 'distant' about $\Delta\varphi \sim 2°$ – thereby reducing the probability of find molecules with a tilt angle in this region. On the other hand, the value of α (or η_A - η_B) in Eq. 9 tends to π/2 faster (when compared to the previous region - φ_{C1}) in this region compensating the decrease in the probability with an increase in the Ω's symmetry (see Eq. 6a-b), rising the transmission function but now for a different reason.

The same explanation can be applied to compare different systems such as C3Bz and C4Bz (see fig. 6c-d). The latter system has just one value in tilt angle (φ=108.18°) where an avoided-crossing occurs around a very small region, but with a value of α (or η_A - η_B) closer to π/2 than for the former. Thus, in this competition, the thermal effect for C4Bz system is less pronounced than for C3Bz since, despite the value of α being closer to π/2 in the A.C. region, the region itself is far from the peak value of $P(\varphi)$ at room temperature, thus covering a small tilt angle region as depicted in figure 6d. This fact diminishes the probability of finding molecules in the A.C. region and, consequently (see table 3), and reduces the increase of the transmission function. This probability of finding molecules in a given tilt-angle region can be quantified by integrating the distribution function around the value φ belonging to an A.C. region and then calculating the weighted average transmission function for the electronic structure at these points. Thus we have:

$$T(E) = P_N T_N(E) + \sum_C P(\varphi_C) T_C(E) \quad , \tag{11}$$

where the indexes C and N, denotes the number of avoided-crossing points and the complementary region, respectively. $P(\varphi_C)$ is the probability to find the system around a given A.C.- tilt angle ($\varphi_C \pm \delta_C$, with δ_C = 0.25° per A.C. point) defined as:

$$P(\varphi_C) = \int_{\varphi_C - \delta_C}^{\varphi_C + \delta_C} P(\varphi) d\varphi \quad . \tag{12}$$

T_C is just the Lorentzian transmission as defined in Eq. 8, with the parameters calculated within the electronic structure at φ_C angle. Finally, T_N and P_N are the transmission function and the probability to find the system out of A.C. regions ($\varphi_C \pm \delta_C$). Thus, for P_N we have $P_N = 1 - \sum_C P(\varphi_C)$ and T_N is the transmission function (Eq. 8) with the parameters calculated out of A.C. regions. Table 3 shows the values for P_N, and $P(\varphi_C)$ for C3Bz and C4Bz.

Table 3: calculated probabilities (Eq. 11)			
System	First A.C. point: $P(\varphi_{C1})$	Second A.C. point: $P(\varphi_{C2})$	P_N
C3Bz	0.093	0.085	0.822
C4Bz	0.041	------	0.959

Using the weights of table 3 and eq. 11 we can insert the avoided-crossing phenomenon due to thermal effects in our model, hence obtaining a mean transmission function that, along with eq.1 results in the electrical current curves shown in figure 7. Such approach effectively explains why at room temperature there is a higher increase in the transmission for C3Bz rather than for C4Bz, thereby flipping the ordering of these systems comparing with the conductivity observed at 6 K: while for C3Bz the first avoided-crossing region almost coincides with its value at room temperature values (of P-M angle), for C4Bz this region is about two degrees (for P-M angle) far from the room temperature situation.

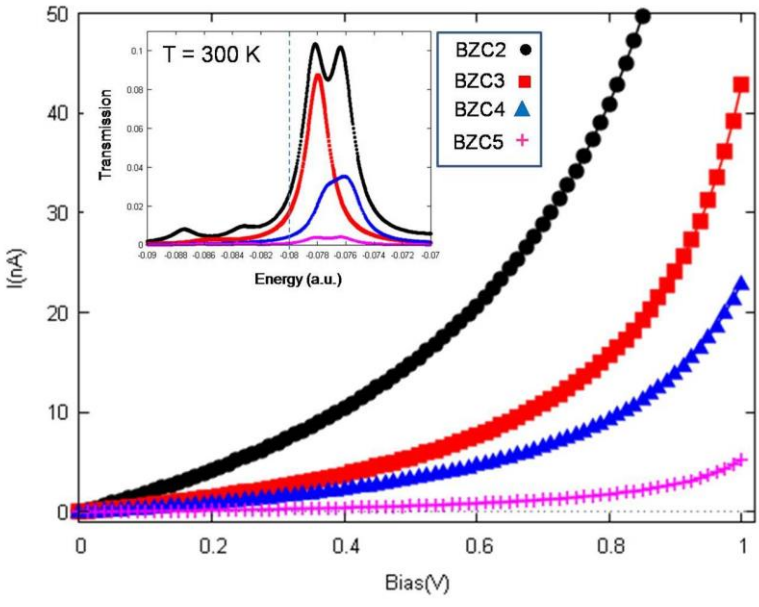

Figure 7: The electrical current for all systems and the transmission function (with the same scale) plotted in the inset for T = 300K.

We stress that the same phenomenon (A.C.) also happens with C5Bz and C2Bz systems (see support information) but the magnitude of the phenomenon (A.C.) is not enough to suppress the exponential decay behavior of the methylenic bridge and change the general trends in the electrical current curve. Moreover, for all systems the AC phenomenon seems to be robust in the sense that it was observed for other functionals (B3PW91) as well (see Supporting Information). Further, the transmission is actually increasing for all systems at higher temperatures, but with different weights. These differences are such that trends of the electrical current between C3Bz and C4Bz systems are flipped, but not for C2Bz and C5Bz. Thus, the avoided-crossing situation due to a small shift in tilt angles seems to be a plausible reason for the inversion in electrical current observed at room temperature.

4. Conclusions.

Using a model self energy (MSE) within a wide band limit approximation (WBL), a theoretical study of charge transport through a nanostructure composed by a methylenic spacer with a phenyl ring connected at the end, attached between a small silicon cluster in the bottom and a small lead cluster at the top, was made within the Non Equilibrium Green's Function theory (NEGF-theory) approach. Treating the electronic structure at the DFT level, together with a molecular dynamics approach to model high temperature effects, we were able to explain two main aspects of these systems, namely how the methylenic bridge containing four carbons conduct better than the bridge with three for cryogenic temperature and why this behavior is flipped at room temperature.

Our results shows qualitative agreement with experimental results [13] showing that, while a geometrical odd-even effect appears at cryogenic temperatures as a geometrical effect where, for even carbons in the methylenic (M) bridge, the barrier between the lead substrate and the phenyl (P) ring is smaller than for the odd case resulting in a more delocalized (localized) molecular orbital for the former (latter), this anomalous feature is suppressed at room temperature. The suppression was explained including the thermal effects within molecular dynamics calculations and incorporating the MD results in ab initio calculations for the room temperature case. In doing this, the

variation in the internal P-M angle φ brings the systems to an avoided crossing (A.C.) region, hybridizing two localized molecular orbitals, and resulting into two new more delocalized ones. Because, at room temperature, the probability of finding the system in the A.C. is higher for *n*-odd (with $n = 3$) than for *n*-even (with $n = 4$), these two systems reverse the behavior of their conductance at cryogenic temperatures.

Our results seem to be robust in the sense that are retrieved also using other DFT functional and thus we believe that, even in its simplicity, the MSE-WBL approach adopted in this work captures the essential physics of the problem.

Acknowledgments: This research was carried out with financial support from Federal University of Pernambuco (Brazil). L. Marques acknowledge the financial support of the Portuguese Foundation for Science and Technology (FCT) in the framework of the Strategic Funding UIDB/04650/2020 and projects SATRAP (POCI-01-0145-FEDER-028108), Control-LUB (UTAP-EXPL/NTec/0107/2017) and Advanced Computing Project CPCA /A2/4628/2020for access to Oblivion HPC resources.

5. References

1. Aviram, A. and M.A. Ratner, *Molecular Rectifiers.* Chemical Physics Letters, 1974. **29**(2): p. 277-283.
2. Remacle, F. and R.D. Levine, *Electrical transmission of molecular bridges.* Chemical Physics Letters, 2004. **383**(5-6): p. 537-543.
3. Larade, B. and A.M.Bratkovsky, *Effect of impurities on transport through organic self-assembled molecular films from first principles.* Physical Review B, 2005. **72**(035440): p. 5.
4. Dalgleish, H. and G. Kirczenow, *Interface states, negative differential resistance, and rectification in molecular junctions with transition-metal contacts.* Physical Review B, 2006. **73**: p. 13.
5. Neel, N., et al., *Conductance of single atoms and molecules studied with a scanning tunnelling microscope.* Nanotechnology, 2007. **18**: p. 4.
6. Mishchenko, A., et al., *Influence of Conformation on Conductance of Biphenyl-Dithiol Single-Molecule Contacts.* Nano Letters, 2010. **10**: p. 8.
7. Thuo, M.M., et al., *Odd-Even Effects in Charge Transport across Self-Assembled Monolayers.* J. Am. Chem. Soc, 2011. **133**: p. 14.
8. Gutiérrez, R., F. Grossmann, and R. Schmidt, *Resistance of Atomic Sodium Wires.* Acta Physica Polonica B, 2001. **32**(2): p. 7.
9. Sim, H.-S., H.-W. Lee, and K.J. Chang, *Even-odd behavior of conductance in monatomic sodium wires.* Physical Review Letters, 2001. **87**(9): p. 4.

10. Smit, R.H.M., et al., *Observation of a Parity Oscillation in the Conductance of AtomicWires.* Physical Review Letters 2003. **91**(7): p. 4.
11. Heimel, G., et al., *Odd-Even Effects in Self-Assembled Monolayers of ö-(Biphenyl-4-yl)alkanethiols: A First-Principles Study*. Langmuir 2008. **24**: p. 9.
12. Akkerman, H.B., et al., *Effects of Odd−Even Side Chain Length of Alkyl-Substituted Diphenylbithiophenes on First Monolayer Thin Film Packing Structure.* J. Am. Chem. Soc, 2013. **135**: p. 9.
13. Toledano, T., et al., *Odd−Even Effect in Molecular Electronic Transport via an Aromatic Ring.* Langmuir, 2014. **30**: p. 10.
14. Havu, P., et al., *Conductance oscillations in metallic nanocontacts.* Physical Review B, 2002. **66**(075401): p. 5.
15. Dubi, Y., *Transport Through Self-Assembled Monolayer Molecular Junctions: Role of In-Plane Dephasing.* J. Phys. Chem. C 2014. **118**: p. 9.
16. Yun, J., et al., *Interesting Odd-Even Effect, Ohmic Contact, Negative Differential Resistance,and Current Stabilizer Behavior in All-Carbon Graphyne/Carbon-Chain Junctions.* IEEE Transactions On Electron Devices, 2020. **67**(6): p. 7.
17. Datta, S., M.A. Ratner, and Y. Xue, *First-principles based matrix Green´s function approach to molecular electronic devices: general formalism* Chemical Physics, 2002. **281**: p. 20.
18. Cuevas, J.C., et al., *Theoretical description of the electrical conduction in atomic and molecular junctions.* Nanotechnology 2003. **14**: p. 10.
19. Datta, S., *Quantum transport: atom to transistor*. 2005, Cambridge, UK ; New York: Cambridge University Press. xiv, 404 p.
20. Di Ventra, M., *Electrical transport in nanoscale systems*. 2008, Cambridge: Cambridge University Press. xvi, 476 p.
21. Juan, E.S. and C. Cuevas, *Molecular Electronics: An Introduction to Theory and Experiment* Nanoscience and Nanotechnology, ed. M. Reed. Vol. 1. 2010: Word Scientific.
22. Datta, S., *Electronic transport in mesoscopic systems*. Cambridge studies in semiconductor physics and microelectronic engineering. 1995, Cambridge ; New York: Cambridge University Press. xv, 377 p.
23. Mingo, N., et al., *Theory of the scanning tunneling microscope: Xe on Ni and Al.* Physical Review B, 1996. **54**(3): p. 11.
24. Verzijl, C.J.O., J.S. Seldenthuis, and J.M. Thijssen, *Applicability of the wide-band limit in DFT-based molecular transport calculations.* The Journal of Chemical Physics, 2013. **138**: p. 11.
25. Moreira, R.A. and C.P. de Melo, *On the separability of the extended molecule: Constructing the best localized molecular orbitals for an organic molecule bridging two model electrodes.* The Journal of Chemical Physics, 2014. **141**(12): p. 124712.
26. Frisch, M.J., et al., *Gaussian 03*, 2004, Gaussian, Inc.: Wallingford CT.
27. Bürkle, M., et al., *Conduction mechanisms in biphenyl dithiol single-molecule junctions.* Physical Review B, 2012. **85**: p. 12.

28. Xiao, L. and L. Wang, *From planar to three-dimensional structural transition in gold clusters and the spin–orbit coupling effect.* Chemical Physics Letters, 2004. **392**: p. 4.
29. Plimpton, S., *Fast Parallel Algorithms for Short-Range Molecular Dynamics.* Journal of Computational Physics, 1995. **117**(1): p. 19.
30. HM Aktulga, e.a., *Parallel reactive molecular dynamics: Numerical methods and algorithmic techniques.* Parallel Computing, 2012. **38**: p. 5.
31. TP Senftle, e.a., *The ReaxFF reactive force-field: development, applications and future directions.* npj Computational Materials, 2016. **2**(15011): p. 14.
32. et-al, F.S., *Si/C/H ReaxFF reactive potential for silicon surfaces grafted with organic molecules.* Journal of Physical Chemistry C, 2018. **122**(41): p. 13.
33. Hoover, W.G., *Canonical dynamics: Equilibrium phase-space distributions. .* Physical Review A, 1985. **31**: p. 3.
34. M, M.P. and A. Rahman, *Polymorphic transitions in single crystals: A new molecular dynamics method. 1981. DOI: 10.1063/1.328693.* Journal of Applied Physics 1981. **52**(12): p. 9.
35. Nozaki, D., H.M. Pastawski, and G. Cuniberti, *Controlling the conductance of molecular wires by defect engineering.* New Journal of Physics, 2010. **12** (063004): p. 20.
36. Ishida, H. and A. Liebsch, *Coulomb blockade and Kondo effect in the electronic structure of Hubbard molecules connected to metallic leads: A finite-temperature exact-diagonalization study.* Physical Review B, 2012. **86**: p. 13.
37. Xu, B. and Y. Dubi, *Negative differential conductance in molecular junctions: an overview of experiment and theory.* Journal of Physics: Condensed Matter, 2015. **27**: p. 19.
38. Szabo, A. and N.S. Ostlund, *Modern quantum chemistry : introduction to advanced electronic structure theory*. 1996, Mineola, N.Y.: Dover Publications. xiv, 466 p.
39. Wang, C.K., Y. Fu, and Y. Luo, *A quantum chemistry approach for current-voltage characterization of molecular junctions.* Physical Chemistry Chemical Physics, 2001. **3**(22): p. 5017-5023.
40. Henderson, T.M., et al., *Determination of complex absorbing potentials from the electron self-energy.* The Journal of Chemical Physics, 2006. **125**: p. 10.
41. Quek, S.Y. and K.H. Khoo, *Predictive DFT-Based Approaches to Charge and Spin Transport in Single-Molecule Junctions and Two-Dimensional Materials: Successes and Challenges.* Accounts of Chemical Research, 2014. **47**: p. 8.
42. Liu, Z.-F. and J.B. Neaton, *Energy-dependent resonance broadening in symmetric and asymmetric molecular junctions from an ab initio non-equilibrium Green's function approach* J. Chem. Phys., 2014. **141**: p. 5.
43. Ojeda, J.H., R.R. Rey-González, and D. Laroze, *Quantum transport through aromatic molecules.* Journal of Applied Physics, 2013. **114**(213702): p. 8.
44. Todd, M.D., A. Nitzan, and M.A. Ratner, *Electron-transfer via Superexchange - a Time-dependent Approach.* Journal of Physical Chemistry, 1993. **97**(1): p. 29-33.

45. Hatton, G.J., *Avoided Crossings of Resonance Energy Curves of One-Electron Atoms in an External Electric-Field.* Physical Review A, 1977. **16**(4): p. 1347-1351.
46. Rotter, I., *Dynamics of quantum systems.* Physical Review E, 2001. **64**: p. 12.
47. Remacle, F. and R.D. Levine, *Level crossing conductance spectroscopy of molecular bridges.* Applied Physics Letters, 2004. **85**(10): p. 1725-1727.
48. Moreira, A.C.L. and C.P. Melo, *Non-Coherent Charge Transport in Donor–Acceptor Systems: A Self-Consistent Description of the Intramolecular Charge Flow*. J. Phys. Chem. C 2012. **116**(4): p. 10.